Numerical analysis of flame shape bifurcation in a two-stage swirled liquid burner using Large Eddy Simulation

Léo C C Mesquita, Aymeric Vié, Laurent Zimmer, Sébastien Ducruix

Numerical analysis of flame shape bifurcation in a two-stage swirled liquid burner using Large Eddy Simulation

Léo C. C. Mesquita[a], Aymeric Vié[a,*], Laurent Zimmer[a], Sébastien Ducruix[a]

[a] *Laboratoire EM2C, CNRS, CentraleSupélec, Université Paris-Saclay, 3 rue Joliot Curie, 91190 Gif-sur-Yvette, France*

Abstract

A flame shape bifurcation in the liquid-fueled two-stage swirled BIMER combustor is studied using Large Eddy Simulations. This combustor, developed at the EM2C Laboratory to study Lean Premixed Prevaporized (LPP) burners, is composed of a two-stage injection system: a central swirled pilot stage fueled with a pressure-swirl atomizer, to sustain a piloting flame, and an outer swirled stage fed with a multi-point injection, to generate the LPP regime. After ignition in the pilot-only operating condition, a V flame is stabilized near the Inner Shear Layer (ISL). When switching to multipoint-only injection, a flame shape transition is observed, and the flame bifurcates into a M-shape. In this work, we identify the mechanisms that lead to this bifurcation, and we show that the transition is driven by a complex coupling between the flame, the chamber acoustics and the ISL vortices. By switching to a multipoint-only injection, the fuel is essentially given to the ISL flame, which is mainly premixed. Because of the increased heat release and

*Corresponding author:
Email address: aymeric.vie@centralesupelec.fr (Aymeric Vié)

thanks to positive Rayleigh criterion, the quarter wave mode of the chamber is promoted. The ISL vortices, locked to this mode, increase in size until they are large enough to merge the flame in the CRZ, because of the radial momentum budget that forces the flow topology to switch to a bubble-like structure. Therefore, these results show that it is the existence of two possible flow topologies that renders this flame shape transition possible, the instability being responsible to transfer sufficient energy to the flow to enable the transitioning and the flame then changing its shape just to adapt to the new topology.

Keywords:
Large Eddy Simulation, Staged combustion, Bifurcation, Combustion instability, Vortices

---

1. Introduction

Lean Premixed Prevaporized (LPP) burners are prone to extinction, flashback or thermo-acoustic instabilities [1, 2]. A candidate for the control of LPP burners is staged injection, which splits the fuel supply in several swirler stages. The two-stage BIMER combustor of EM2C laboratory has been developed to expand the knowledge on LPP staged burners.It is composed of an outer stage fed with a multipoint injection system, which goal is to generate the LPP regime thanks to fast atomization and evaporation; and of a central stage fueled with a pressure-swirl atomizer that sustains a rich diffusion-like pilot flame close to the injection system, aiming to stabilize the burner operation [3, 4].

Thanks to the versatility of this staged injection system, thermo-acoustic

instabilities and flame shape bifurcations can be triggered and studied depending on the injection regime and a hysteretic behaviour can lead to multistable operating points. Indeed, experimental and numerical studies have exhibited three flame archetypes and three bifurcations between these flames when varying the fuel distribution between the stages [3–8]: a V-flame, an M-flame and a Tulip-flame. In [4, 6], the authors studied two of these flame shape bifurcations. Starting from a V-flame with dual injection and ceasing to feed the pilot injector with fuel leads to an M lifted flame. Reinjecting fuel from the pilot burner recovers the V-flame by flashback. In [7], this transition has been numerically evidenced for the operating conditions of [3] and some mechanisms have been suggested to explain it. Here, the objective of this study is to investigate further the mechanisms driving this type of transition using an updated LES numerical setup with a finer mesh and a Lagrangian description for the liquid fuel to better reproduce the phenomena observed experimentally in [5]. Compared to [7], we focus on the operating conditions of [4–6], for which a similar transition is observed and a larger set of validation data is available.

This paper is organized as follows. First, the combustor and the operating conditions are presented. The numerical setup is showed and a brief description of the flame ignition and initialization is given. Finally, the transition results are presented, and the main events and mechanisms controlling the transition are discussed.

2. Description of the setup

2.1. Experimental setup and operating conditions

BIMER is a labscale combustor designed to investigate the operation of a swirling two-stage injector. An inlet feeding line leads the air to a cylindrical plenum, which passes through the injection system and then reaches a rectangular combustion chamber ($500 \times 150 \times 150 mm^3$). The chamber contains three water-cooled walls (entrance, top and bottom) and two large lateral silica windows for optical access. The swirling injector is composed of two stages (Fig. 1): the central stage is called the pilot stage. Including a pressurized nozzle it creates a hollow cone of droplets with a spray half angle of 30°. It naturally admits approximately 15 % of the total air mass flow rate, and a geometric swirl number of 0.6 is imposed. The main external stage is called the multipoint stage, as fuel is injected through 10 holes of 0.3 mm diameter, placed at the second swirler vanes exits to perform a jet in cross-flow injection and improve mixing. This stage admits 85 % of the air mass flow rate, imposing a geometric swirl number of 1.

The operating conditions match the experimental data of Renaud [5]. The burner operates at atmospheric pressure, with an air mass flow rate of 43 $g.s^{-1}$ preheated at 433K, and a total fuel mass flow rate of 1.64 $g.s^{-1}$, leading to a global equivalence ratio of 0.6, and a thermal power close to 73 kW. These parameters are kept constant, while the fuel distribution between the stages varies. This variation is measured by the staging factor α, which is the ratio between the fuel mass flow rate injected through the pilot stage and the total fuel mass flow rate. The staging factor is varied from 15% to 0%.

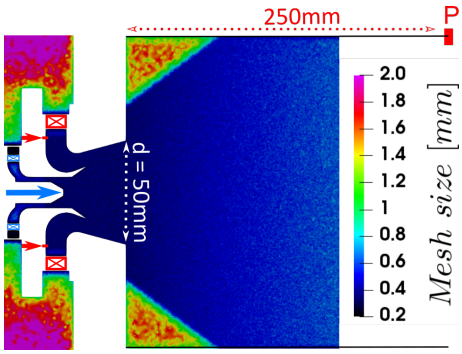

Figure 1: XZ plane view of the injector at the entrance of the combustion chamber colored by the mesh size. Cyan crosses and arrow indicate, respectively, the pilot swirlers and injector, while the red crosses and red arrows indicate respectively multipoint swirlers and two multipoint injection holes (out of scale). The pressure probe is identified by a red rectangle. Flow from left to right.

2.2. Numerical setup

AVBP, an unstructured code co-developed by CERFACS and IFPEN [9] that solves the 3D compressible reacting multi-species Navier-Stokes equations, is used. The LES sub-grid scales are modeled using the WALE model [10]. A 3^{rd} order in time and space Two-step Taylor-Galerkin (TTGC) scheme is used. Artificial diffusion is implemented to treat numerical perturbations and stiff gradients [11]. Gaseous inlet and outlet are treated with the Navier-Stokes Characteristic Boundary Conditions (NSCBC)[12]. Walls are considered as non-slipping and adiabatic, except for the two water-cooled walls which are treated as isothermal.

A Lagrangian modeling is used for the liquid phase, using one numerical parcel per physical droplet. Droplet diameter distributions have been extracted from experimental studies [5] for both stages. Evaporation is mod-

eled with the Abramzon-Sirignano model [13]. Details of the implementation can be found in [14]. Interaction of droplets with the walls is set to slip. This aims at reproducing in a very simplistic way a film-like behavior at the divergent exit observed in the experiments [5]. This setup and the injection strategy for the pilot spray were validated in [15]. The chemistry is described by the BFER reduced scheme for kerosene [16], under the unity Lewis number assumption, and the flame-turbulence interaction is treated using the Thickened Flame model (TFLES) [17], where flame wrinkling is calculated using Charlette's formalism [18]. An unstructured mesh composed of 132 million tetrahedra is used (elements size can be seen in Fig. 1), keeping the thickening factor between 3 and 7.

2.3. Initialization procedure

To reproduce the experimental procedure, the flame is ignited at a pilot-only injection condition ($\alpha = 100\%$), which generates a V-shaped flame. From this state, the fuel staging is slowly modified, changing α at the rate of 1% per millisecond of simulated physical time, until α reaches the value of 15%. The resulting V-shaped flame at $\alpha = 15\%$ is shown in Fig. 2a and presents two main features: (1) a rich diffusion flame downstream the pilot injector mostly burning in a diffusion regime, characterized by a strong interaction between spray and flame and associated with high temperatures (around 2300K); and (2) further downstream, the remaining of the flame burning mostly premixed close to the global equivalence ratio, leading to lower temperature, near 1600K, confirming the observations made in [7]. This premixed flame is stabilized on the Inner Shear Layer (ISL) between the fresh and burned gases and the V-shape of the flame is linked with

the flow topology created by the Conical Vortex Breakdown, present in this condition. Thus, the Central Recirculation Zone (CRZ) is large and open, starting upstream the pilot injection and reaching the center of the chamber.

3. Analysis of the flame shape transition

From the stable V state, α is reduced from 15% to 0% at a rate of 1% per ms, meaning that the pilot injection is progressively decreased as the multipoint injection is increased. In the following, the transition is carefully analyzed and the phenomena at stake are identified.

3.1. Flame shape evolution

In Fig. 2, the flame shape evolution is presented from the initial V-state to the final M-state. Between Fig. 2a and 2b, the pilot injection has been stopped (at $t = 15ms$) and the portion of the flame anchored by the central spray extincts. In Fig. 2b, a large toroidal vortex is visible (identified by arrows), increasing in size in the middle of the flame, in the portion stabilized at the ISL. These large vortices, not observed during the initial V state, occur at the axial position of the CRZ bubble contraction (Fig. 2b). They are directed inwards, leading to a strong oscillation of the inner flame and CRZ diameters. This first vortex is convected downstream, restoring the flame to its original shape and showing a periodic oscillatory behavior. In the following period (Fig. 2c), a new vortex, subsequent to that in Fig. 2b, starts forming. This vortex pushes the inner flame and CRZ inwards even further (Fig. 2d). However, this time, they do not recover their original diameter after the vortex is convected downstream. In the following period, a third vortex arrives and becomes large enough to further push the inner

flame inside the CRZ and contract its diameter down to zero, leading to the flame merging in the CRZ (Fig. 2e). The flame is then separated into two parts by the vortex and each one evolves independently: an internal flame, once stabilized over the ISL is blown towards the pilot injector by the CRZ negative velocity (Fig. 2e) and eventually extinguishes (Fig. 2f); and an external flame, anchored at the OSL, keeps this anchoring and crosses the CRZ (as a consequence of the transition), and stabilize its leading edge at the CRZ's contraction and to take the final M-shape (Fig. 2f).

The final M flame is shown in Fig. 2f. It is completely stabilized inside the combustion chamber, burning mostly in lean premixed regime, with a lower temperature near 1600K. After the transition, the flow topology returns to the original non-reactive one: instead of the large open recirculation zone, the CRZ has a round bubble-like shape, characteristic of the Bubble Vortex Breakdown. The CRZ is filled with fuel vapor and air coming from the multipoint stage, which mixes with air coming from the pilot stage to produce a mixture close to the global equivalence ratio. A pressure drop at the CRZ is also observed, like in non-reacting conditions. The flame is stabilized by the OSL and the leading point is localized at the bottle-neck region of the CRZ, where the fresh gases reenter the CRZ and quenches the flame, preventing it to propagate and burn the mixture inside the CRZ.

3.2. Combustion instability and inner flame evolution

The acoustic activity inside the combustion chamber (Fig. 3.a) shows that, as soon as the pilot injection starts being reduced ($t = 0$ ms), the pressure fluctuations increase, reaching the maximum amplitude at the flame transition and, then, decreases. This pressure oscillation is in phase with the

global heat release rate, meaning that the Rayleigh criterion is fulfilled and that a thermo-acoustic instability occurs, locked on the longitudinal quarter-wave mode of the chamber (with a characteristic frequency of around 290 Hz [5]). This increase in thermo-acoustic activity is due to the change in fuel distribution and the fact that the flame now features LPP characteristics. These points will be addressed in more detail in the next section.

Simultaneously with the increase in acoustic and heat release rate oscillations, a larger flame surface oscillation is visible as the pilot injection is stopped (Fig. 3.b). The maxima of the flame surface evolution coincide with the presence of the toroidal vortices shown in Fig. 2, linking these vortices, which are at the origin of the contraction of the inner flame and of the transition, with the heat release rate oscillations. Therefore, to better study the flame shape transition, the evolution in time of the inner flame, defined as the portion of the flame that is stabilized over the ISL (as seen in Fig. 2), is closely observed. To analyze the evolution of its diameter, the inner flame is approximated by a circle, which has been verified as a reasonable assumption because of its axisymmetry. The beginning of the transition is clearly identified by the fast contraction of the ellipse at $t = 15\ ms$, synchronized with the CRZ diameter contraction, attesting that both evolve very similarly.

3.3. Inner flame and ISL vortices dynamics

It is now clear that this transition is driven by the inner flame evolution and the way it interacts with the acoustic mode and the inner shear layer. However, the phenomena involved here seem different from the classical driving mechanisms usually generating heat release rate fluctuations in premixed swirling flames subjected to incident acoustic perturbations. Here, the typ-

ical flame tip roll-up [19] with a rotation direction from the center to the outwards of the chamber is not observed. Alternatively, as shown in Fig. 2b, a vortex rotating inwards is observed at the center of the flame, and not at its tip. It is rather the interaction between the acoustic mode and the ISL helical vortices that drives the dynamics in heat release rate oscillations by wrinkling the flame. Such mechanisms were also observed and analyzed by [20–22] in premixed lifted methane flames.

In the BIMER combustor, when the staging factor is decreased from α=15% to 0%, 15% of the fuel mass flow rate is redirected towards the multipoint injection. This changes the spatial distribution of fuel in the chamber as visible in Fig. 2, transferring fuel from the central nozzle spray region to the ISL region. As the flame must adapt to this new distribution, the flame front moves from a region burning in a stable rich diffusion regime to another where it is lean, premixed and strongly interacting with the ISL. Figure 3.a shows the evolution of the heat release rate as a function of time during the transition. One clearly observes a change in amplitude of oscillations of the heat release rate and of the flame surface at $t = 6$ ms, after the change in staging is initiated. This is then followed by an increase in acoustic pressure oscillations. This increase in the (longitudinal) acoustic pressure oscillations leads to axial velocity oscillations that excite the helical vortices in the ISL, probably associated with Kelvin-Helmholtz hydrodynamic instabilities. This can be particularly seen in Fig.4, where the evolution of positive axial velocity in the jet entering the chamber and of negative velocity inside the CRZ are plotted simultaneously with the CRZ diameter. Indeed, before $t = 15$ ms, both velocities and the CRZ diameter are oscillating in phase. Thus, when

the axial velocity increases due the passage of the acoustic wave, the CRZ diameter also increases and the jet (and flame), then, opens, corresponding to the classical flame opening oscillations found in swirled flames subject to acoustic oscillations [19]. Nonetheless, after $t = 15$ ms, when the staging factor reaches zero and the toroidal vortices at the ISL begin to increase in size (as shown in Fig. 2), the velocities and the CRZ diameter begin to evolve in phase opposition. Therefore, as the acoustic pressure wave passes, it increases both positive axial velocity in the fresh gases jet and the negative velocity in the CRZ, but this now leads to the increase in the size of the toroidal vortex at the ISL, that pushes the CRZ inwards, reducing its diameter. The toroidal vortex is then the link between the axial velocity oscillations and the opposite variation of the CRZ diameter.

To understand how the acceleration of the flow by the acoustic pressure wave leads to the creation of the toroidal vortex at the ISL, the ISL dynamics in the initial stable case (α=15%) is analyzed. Studying the stable V flame at α=15% one can better observe how the vortices are formed and how they interact between themselves, with the flame, and with the pressure and flow oscillations due to the acoustics. Figure 5 zooms in the divergent region, focusing on the ISL helical vortices. As these vortices are convected downstream by the flow and an acoustic pressure wave passes (accelerating the flow accordingly), the helical vortices tend to merge until they create a larger vortex, locked on the acoustic frequency, as shown in Figure 5. See [23] and references therein for details on this mechanism. With the triggering of the combustion instability due to the change on the staging factor and continuous increase in acoustic pressure amplitude, this merging of helical

vortices is intensified, thus creating the toroidal vortices shown in Fig. 2 that will lead to the flame shape transition.

Regarding the interaction between the ISL vortices and the flame, in Fig. 5, it is possible to see how the ISL helical vortices wrinkles the flame, especially on the top part of the figure. Therefore, changing the staging factor to α=0% will increase the quantity of fuel over the ISL and, thus, the heat release rate of the premixed flame over the ISL. This will naturally result in the increase of the heat release rate oscillations, due to the natural wrinkling the flame caused by the ISL helical vortices. And, as the combustion instability leads to the merging of the helical ISL vortices in a large toroidal vortex, the later increases even more the wrinkling, re-increasing the acoustic pressure oscillations and closing the coupling mechanism of the instability. The occurrence of the toroidal vortices matches the flame surface variations (as shown in Fig 3), showing their role in altering the flame surface and modifying the heat release rate. This seems to be a case of a classical vortex-driven instability [1, 24], but in a swirled ISL stabilized flame, where the heat release rate fluctuates due to vortex driven flame wrinkling [20–22].

3.4. Changes in flow topology

As the vortices grow, they push the CRZ limits inwards. Figure 6.a presents the time evolution of the CRZ radius at a distance $x = 0.015\ m$ from the chamber entrance. As already discussed, before the transition, the CRZ radius slightly oscillates, because of the ISL vortices and the flow angle oscillations due to the interactions between the acoustic fluctuations and the swirler [19]. By this mechanism, the flame is expected just to oscillate around its stable opening, however, after the pilot injection is stopped, the radius of

the CRZ progressively decreases and the transition occurs.

One key question is why do this progressive reduction occurs? The increasingly large toroidal vortices do not explain the CRZ being progressively reduced, they should only act as an oscillating mechanism, pushing the CRZ inwards, that would afterwards return to its original diameter. However, after reaching a certain value, the CRZ radius inevitably decreases and leads to the change in flow topology. The flow is forced to move from a stable topology to another stable one, by gathering sufficient energy from the vortices responsible for the transition. Below is proposed a discussion on a possible mechanism causing the flow topology bifurcation.

The toroidal vortices push the CRZ, consequently reducing its radius and, thus, the incoming fresh gases jet radius, as one can see on the image sequence of Fig. 2. Considering angular momentum conservation, the reduction of the radius of rotating annular mass implies an increase in angular velocity. Figure 6.b confirms this behavior, as the angular velocity increases in magnitude following the radius reduction. To understand how the swirling flow dynamics affect the radial velocity u_r, the radial momentum conservation is analyzed. When dealing with vortex breakdown, the centrifugal force and radial depression terms are commonly considered as the most relevant ones for the radial velocity budget ([25, 26]). This same assumption is used here.

Back to the transition study, CRZ radius reduction and the swirling velocity increase imply an augmentation of the centrifugal force. As a consequence, due to radial momentum conservation, when reaching a critical radius value, this increase in centrifugal force causes an increase in radial

pressure gradient. This creates a new equilibrium state for the system, stabilizing the CRZ at the current reduced diameter and not returning the CRZ to its original diameter. The difference between centrifugal force and radial pressure gradient is overall positive until $t = 20ms$ (Fig. 6c), when the toroidal vortices are large enough to start pushing the CRZ inwards. From this point on, approximately $3ms$ before the transition instant (when the swirling velocity reaches the maximum absolute value before the transition), the difference between centrifugal force and radial pressure gradient becomes negative (Fig. 6c), creating a depression inside the CRZ and progressively reducing the radial velocity component (Fig. 6d). These phenomena still evolve until the CRZ diameter reaches the non-reacting CRZ diameter, then the pressure drop pull combined with the final vortex push are responsible for deviating part of the fresh gas jet inside the CRZ and recreating the fresh gas bubble seen in the non-reacting case. This pushes the flame inwards and changes the flow topology from a conical vortex breakdown to a bubble vortex breakdown and the flame shape from a V-ISL-stabilized-shape to an M-shaped flame stabilized by the OSL and the vortex breakdown bubble.

4. Conclusion

The LES of a two-stage swirl stabilized liquid-fueled burner have been performed to analyse a singular flame shape transition. This transition is triggered by a change in the injection regime to make the burner operate in LPP conditions. A strong coupling between flame, acoustics and flow dynamics is observed, creating an intricate mechanism. Changing the spatial distribution of fuel triggers a combustion instability, due to the wrinkling

of the flame caused by the ISL helical vortices. The increase in acoustic oscillations will favor the natural merging of the ISL helical vortices to create a large toroidal vortex. This vortex then wrinkles more the flame, increasing the amplitude of the instability and closing the loop. This phenomenon self-amplifies at each iteration until a sufficiently large toroidal vortex completely contracts the inner flame, pushes the CRZ inwards and deviates the fresh gases jet inside the CRZ. This causes the flow topology to change from a conical Vortex Breakdown to a Bubble Vortex Breakdown and, thus, the flame to transition from a V-shaped to M-shaped flame. It is, hence, the existence of two possible flow topologies in this burner that will ultimately be the reason for the flame shape transition. The instability triggers the mechanism responsible to transfer enough energy to the flow, enabling it to change its topology. The flame shape changes, then, just to adapt to this new flow topology. The non-existence of multiple possible flow topologies should, therefore, be verified as a primary condition to avoid this type of transition.

Acknowledgments

We thank CERFACS for sharing the AVBP solver. This work was granted access to the HPC resources of CINES under the allocation A0012B00164 made available by GENCI, and of the mesocentre computing center of CentraleSupélec and Ecole Normale Supérieure Paris-Saclay supported by CNRS and Region Ile-de-France (http://mesocentre.centralesupelec.fr/).

References

[1] S. Ducruix, T. Schuller, D. Durox, S. Candel, Combustion dynamics and instabilities: Elementary coupling and driving mechanisms, J. Prop. Power 19 (2003) 722–734.

[2] T. Lieuwen, V. Yang (Eds.), Combustion Instabilities in Gas Turbine Engines: Operational Experience, Fundamental Mechanisms, and Modeling, volume 210, Prog. in Astronautics and Aeronautics , 2005.

[3] T. Providakis, L. Zimmer, P. Scouflaire, S. Ducruix, Characterization of the coherent structures in swirling flames stabilized in a two-stage multi-injection burner: influence of the staging factor, C. R. Acad. Sci. 341 (2013) 4–14.

[4] A. Renaud, S. Ducruix, P. Scouflaire, L. Zimmer, Flame shape transition in a swirl stabilised liquid fueled burner, Proc. Combust. Inst. 35 (2015) 3365–3372.

[5] A. Renaud, High-speed diagnostics for the study of flame stabilization and transient behaviour in a swirled burner with variable liquid-fuel distribution, Ph.D. thesis, CentraleSupélec, 2015.

[6] A. Renaud, S. Ducruix, L. Zimmer, Bistable behaviour and thermoacoustic instability triggering in a gas turbine model combustor, Proc. Combust. Inst. 36 (2017) 3899–3906.

[7] B. Cheneau, A. Vié, S. Ducruix, Characterization of the hysteresis cycle in a two-stage liquid-fueled swirled burner through numerical simulation, Proc. Combust. Inst. 37 (2019) 5245–5253.

[8] B. Cheneau, A. Vié, S. Ducruix, Numerical study of flame shapes and structures in a two-stage two-injection aeronautical burner with variable fuel staging using eulerian large eddy simulations, J. Eng. Gas Turb. and Power 141 (2019).

[9] L. Gicquel, G. Staffelbach, T. Poinsot, Large eddy simulations of gaseous flames in gas turbine combustion chambers, Prog. Energy Comb. Sci. (2012).

[10] F. Nicoud, F. Ducros, Subgrid-scale stress modelling based on the square of the velocity gradient tensor, Flow, Turb. and Combustion 62 (1999) 183–200.

[11] O. Colin, M. Rudgyard, Development of high-order taylor-galerkin schemes for les, J. Comput. Phys. 162 (2000) 338 – 371.

[12] T. Poinsot, S. Lele, Boundary conditions for direct simulations of compressible viscous flows, J. Comput. Phys. 101(1) (1992) 104–129.

[13] B. Abramzon, W. Sirignano, Droplet vaporization model for spray combustion calculations, Int. J. Heat and Mass Transfer 32 (1989) 1605–1618.

[14] G. Hannebique, P. Sierra, E. Riber, B. Cuenot, Large eddy simulation of reactive two-phase flow in an aeronautical multipoint burner, Flow, Turb. and Combustion 90 (2013) 449–469. 10.1007/s10494-012-9416-x.

[15] L. C. C. Mesquita, A. Vié, S. Ducruix, in: Proceedings of the ASME Turbo Expo 2018, Oslo, Norway.

[16] B. Franzelli, E. Riber, M. Sanjosé, T. Poinsot, A two-step chemical scheme for kerosene–air premixed flames, Combust. Flame 157 (2010) 1364 – 1373.

[17] P. Poinsot, D. Veynante, Theoretical and Numerical Combustion, e-learning@CERFACS, Third Edition, 2012.

[18] F. Charlette, C. Meneveau, D. Veynante, A power-law flame wrinkling model for LES of premixed turbulent combustion part II: dynamic formulation, Combust. Flame 131 (2002) 181 – 197.

[19] S. Candel, D. Durox, T. Schuller, J. Bourgouin, J. P. Moeck, Dynamics of swirling flames, Ann. Rev. Fluid Mech. 46 (2014) 147–76.

[20] V. Caux-Brisebois, A. Steinberg, C. M. Arndt, W. Meier, Thermo-acoustic velocity coupling in a swirl stabilized gas turbine model combustor, Combust. Flame 161 (2014) 3166–3180.

[21] A. M. Steinberg, I. Boxx, M. Stohr, C. D. Carter, W. Meier, Flow-flame interactions causing acoustically coupled heat release fluctuations in a thermo-acoustically unstable gas turbine model combustor, Combust. Flame 157 (2010) 2250–2266.

[22] A. M. Steinberg, I. Boxx, M. Stohr, W. Meier, C. D. Carter, Effects of flow structure dynamics on thermoacoustic instabilities in swirl-stabilized combustion, AIAA Journal 50 (2012) 952–967.

[23] T. C. Lieuwen, Unsteady Combustor Physics, Cambridge University Press, 2012.

[24] T. Poinsot, A. Trouve, D. Veynante, S. Candel, E. Esposito, Vortex-driven acoustically coupled combustion instabilities, J. Fluid Mech. 177 (1987) 265–292.

[25] O. Lucca-Negro, T. O'Doherty, Vortex breakdown: a review, Prog. Energy Comb. Sci. 27 (2001) 431–481.

[26] E. Krause, A contribution to the problem of vortex breakdown, Computers and Fluids 13 (1985) 375–381.

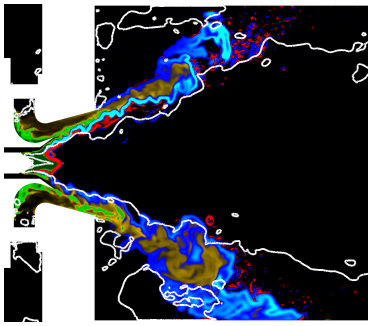

(a) t = 0 ms: V flame @ α = 15%

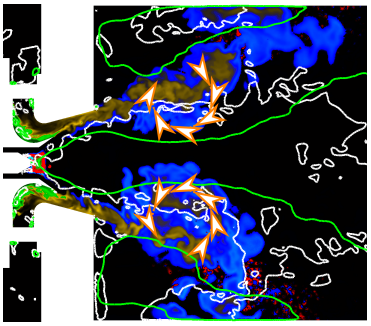

(b) t = 17.6 ms: 2.6ms after α reaches 0%, the first large vortex appears and afterwards dissipates

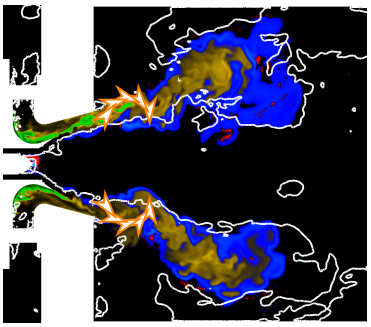

(c) t = 19.8 ms: a second large vortex starts forming

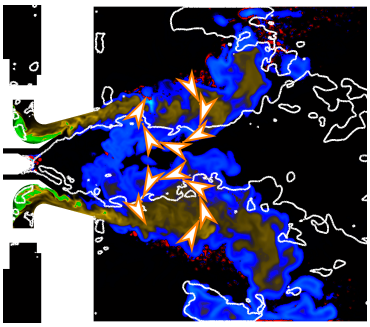

(d) t = 21.4 ms: a second large vortex pushes inner flame and CRZ inwards, that don't return to original diameter

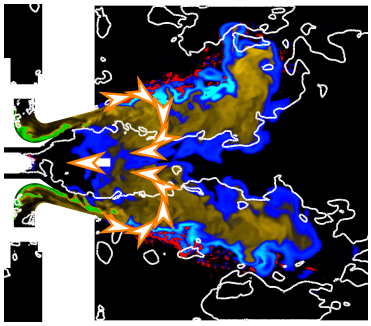

(e) t = 23.1 ms: a third vortex pushes flow inwards even further, collapsing the inner flame, that cuts and is convected upstream by the CRZ

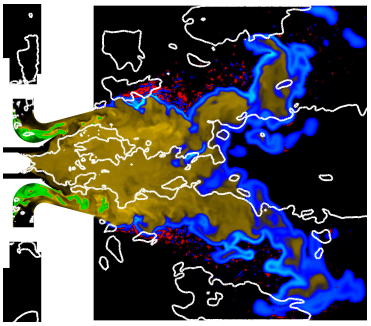

(f) t = 50.0 ms: M flame @ α = 0%

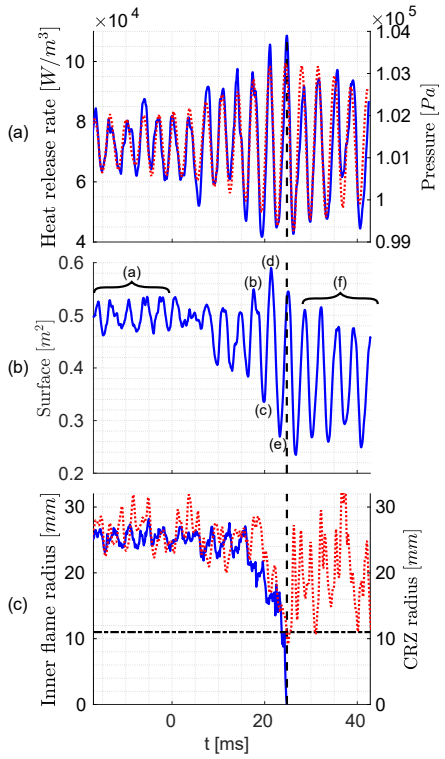

Figure 3: (a) time evolution of the integrated heat release rate (red) and the pressure (blue), measured by a probe at the experimental microphone position at (x,y,z)=[0.25, 0, 0.075]m. (b) time evolution of heat release rate iso-surface at a value of $10^7 W$ level. The letters correspond to the flames shown in Fig. 2. The vertical black line indicates the transition instant. (c) Time evolution of the equivalent radius of the interpolated circle over the inner flame at position X=0.03m (blue). The data stops when the circle diameter reaches zero, moment defined as flame shape transition. The CRZ radius (dotted red line) indicates the correlation between the inner flame and the CRZ. The dot-dashed horizontal line indicates the average CRZ radius for the M flame at this position.

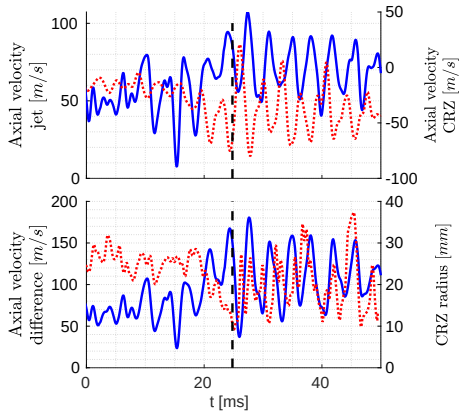

Figure 4: Top: evolution in time of axial velocity measured in the fresh gases jet @ x=0.015mm and z=0.025mm (blue) and axial velocity measured inside the CRZ @ x=0.015mm and z=0.000mm (dotted red). Bottom: difference between the two aforementioned axial velocity measurements (blue) and CRZ diameter measured @ x=0.015mm (dotted red).

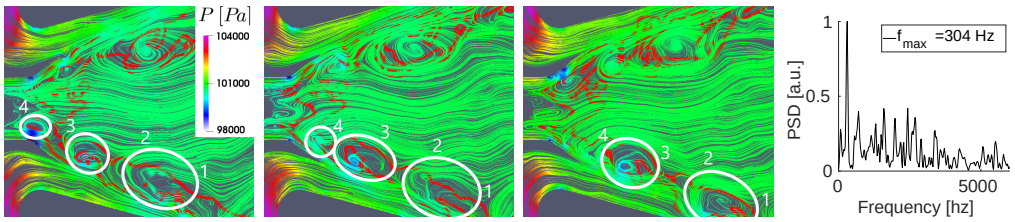

(a) t = 25.4 ms (b) t + 0.1ms (c) t + 0.2ms (d) PSD

Figure 5: (a,b,c) XZ plane instantaneous snapshots of the pseudo-streamlines colored by the pressure showing the vortex-merging in the ISL of the stable V flame. Red lines represent the iso-contour of heat release rate at $10^7 W/m^3$. (d) Normalized PSD of the Q-criterion measured at the position of the vortex 1+2 in (c). Acquisition frequency and time of 10^5 Hz and 40 ms; PSD performed with the Welsh method with 2 equal length Hanning windows.

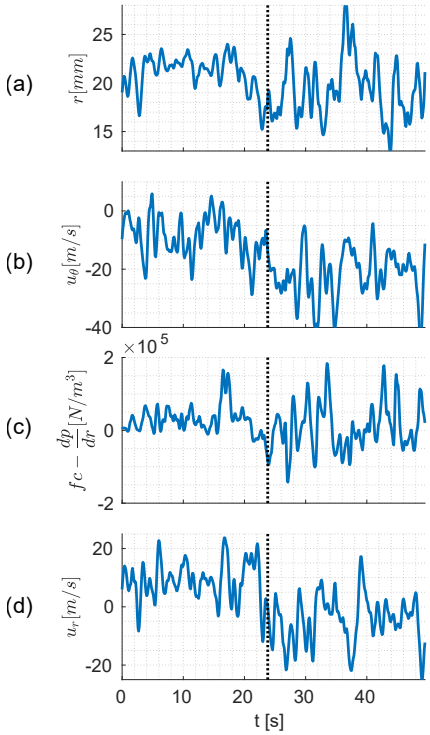

Figure 6: Dynamics of a point over the CRZ at x=0.015 m: (a) CRZ radius, (b) velocity swirl component, (c) balance between centrifugal force and pressure radial gradient, (d) velocity radial component. Signals are filtered with a 4th order Butterworth low-pass filter and a frequency cut at 600Hz. The dashed vertical line identifies the moment at which the inner flame has merged in the CRZ.